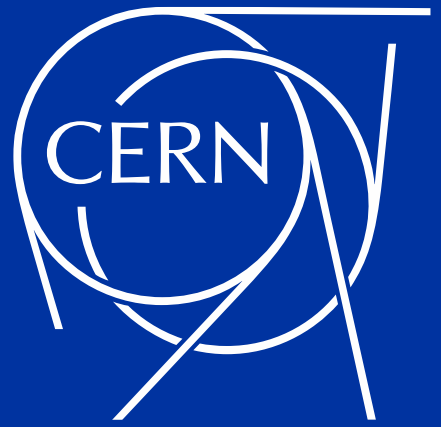

High-Gradient Testing of NCRF Materials

Lee Millar[1]

[1]CERN SY-RF-SRF

Materials for Bright Beams Workshop 2025

Cornell University, Ithaca, New York, USA

Introduction

The objective of this presentation – to survey some of the key observations and scaling laws related to arcing which have emerged from high-gradient tests, with reference to a variety of experiments and publications.

This presentation is entirely subjective, and non-exhaustive! An enormous amount of work has been conducted to date, so I will superficially cover only few topics and generally focus on the empirical side of things. To start off, a little bit of history…

Back to the start…

1924 – The first proposal*.

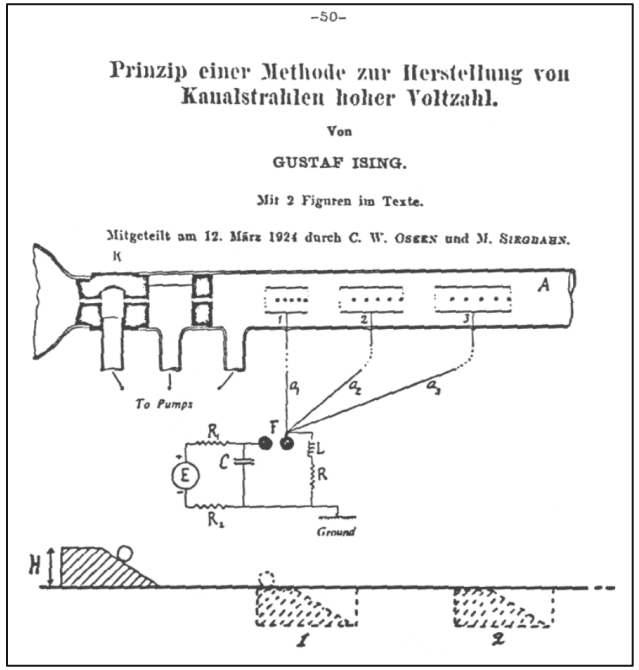

–50–

Prinzip einer Methode zur Herstellung von Kanalstrahlen hoher Voltzahl.

Von

GUSTAF ISING.

Mit 2 Figuren im Texte.

Mitgeteilt am 12. März 1924 durch C. W. OSEEN und M. SIEGBAHN.

G. Ising, Prinzip einer Methode zur Herstellung von Kanalstrahlen hoher Voltzahl, ser. Arkiv för matematik, astronomi och fysik. Almqvist & Wiksells BoktryckeriA.B., 1924, translated as: *Principle of a method for the Production of Canal Rays of High Voltage.*

A few years later…

1928 – The first implementation.

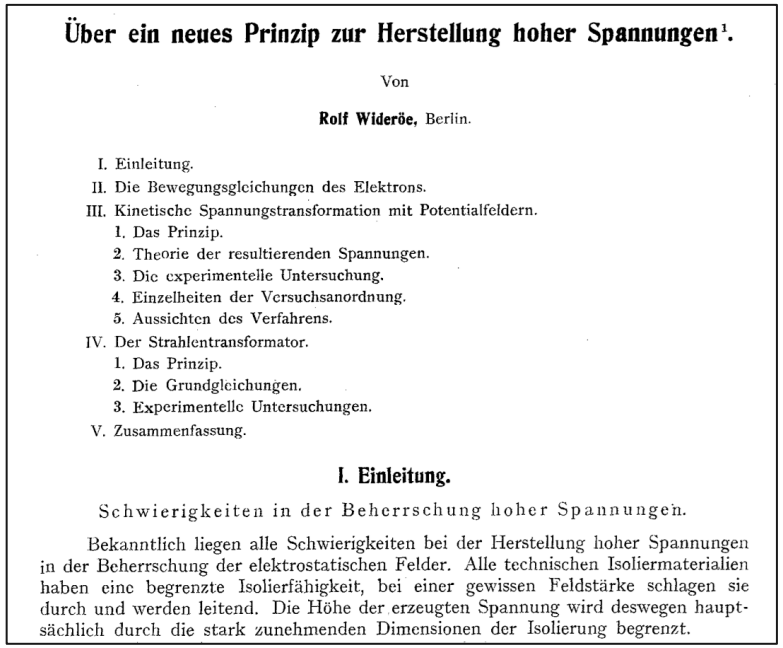

Über ein neues Prinzip zur Herstellung hoher Spannungen[1].

Von

Rolf Widerøe, Berlin.

I. Einleitung.

Schwierigkeiten in der Beherrschung hoher Spannungen.

Bekanntlich liegen alle Schwierigkeiten bei der Herstellung hoher Spannungen in der Beherrschung der elektrostatischen Felder. Alle technischen Isoliermaterialien haben eine begrenzte Isolierfähigkeit, bei einer gewissen Feldstärke schlagen sie durch und werden leitend. Die Höhe der erzeugten Spannung wird deswegen hauptsächlich durch die stark zunehmenden Dimensionen der Isolierung begrenzt.

R. Widerøe, "Über ein neues Prinzip zur Herstellung hoher Spannungen", Arch. Elektrotech., vol. 21, pp. 387–406, 1928, translated as*: A new principle for the generation of high voltages.*

*Image of the publication taken from a CERN Accelerator School talk by Philip John Bryant: https://cas.web.cern.ch/sites/default/files/lectures/granada-2012/bryant.pdf

Back to the start…

1924 – The first proposal*.

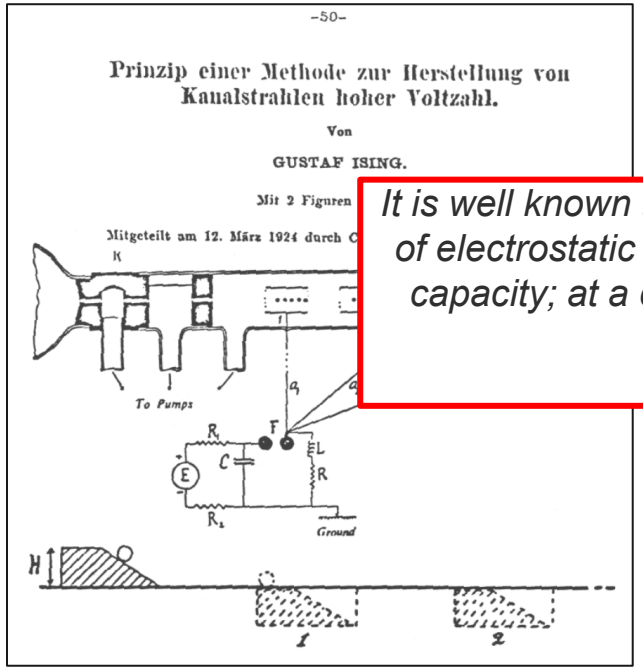

–50–

Prinzip einer Methode zur Herstellung von Kanalstrahlen hoher Voltzahl.

Von

GUSTAF ISING.

Mit 2 Figuren

Mitgeteilt am 12. März 1924 durch C

K

To Pumps

R

F

C

EL

R

E

R_1

Ground

H

1

2

G. Ising, Prinzip einer Methode zur Herstellung von Kanalstrahlen hoher Voltzahl, ser. Arkiv för matematik, astronomi och fysik. Almqvist & Wiksells BoktryckeriA.B., 1924, translated as: ***Principle of a method for the Production of Canal Rays of High Voltage.***

It is well known that all the difficulties in producing high voltages lie in the control of electrostatic fields. All technical insulating materials have a limited insulating capacity; at a certain field strength they break down and become conductive.

- R. Widerøe (1928) [translated from German].

1928 – The first implementation.

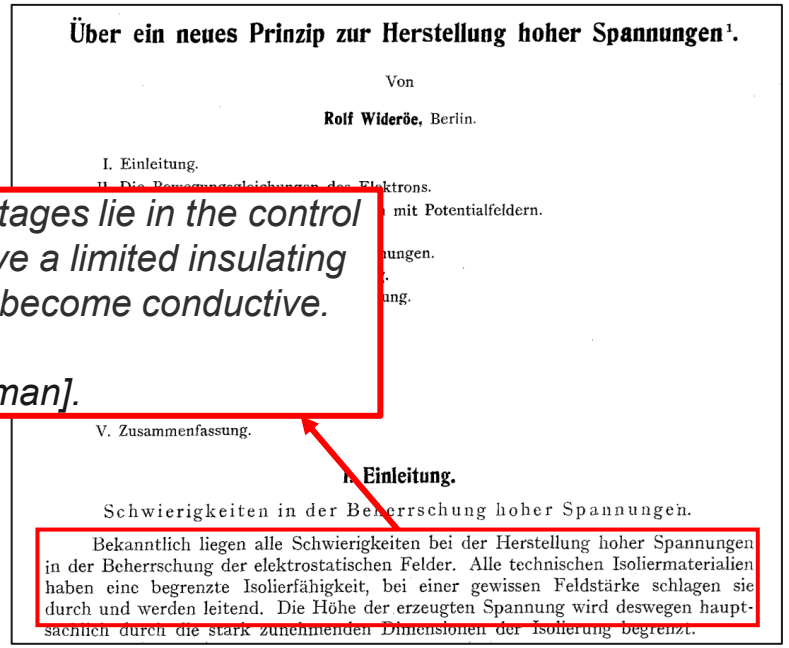

Über ein neues Prinzip zur Herstellung hoher Spannungen[1].

Von

Rolf Wideröe, Berlin.

I. Einleitung.

mit Potentialfeldern.

V. Zusammenfassung.

I. Einleitung.

Schwierigkeiten in der Beherrschung hoher Spannungen.

Bekanntlich liegen alle Schwierigkeiten bei der Herstellung hoher Spannungen in der Beherrschung der elektrostatischen Felder. Alle technischen Isoliermaterialien haben eine begrenzte Isolierfähigkeit, bei einer gewissen Feldstärke schlagen sie durch und werden leitend. Die Höhe der erzeugten Spannung wird deswegen haupt-

R. Widerøe, "Über ein neues Prinzip zur Herstellung hoher Spannungen", Arch. Elektrotech., vol. 21, pp. 387–406, 1928, translated as*: A new principle for the generation of high voltages*.

*Image of the publication taken from a CERN Accelerator School talk by Philip John Bryant: https://cas.web.cern.ch/sites/default/files/lectures/granada-2012/bryant.pdf

Towards the State of the Art

Facilities all over the globe investigate the limitations on the achievable field for a variety of applications.

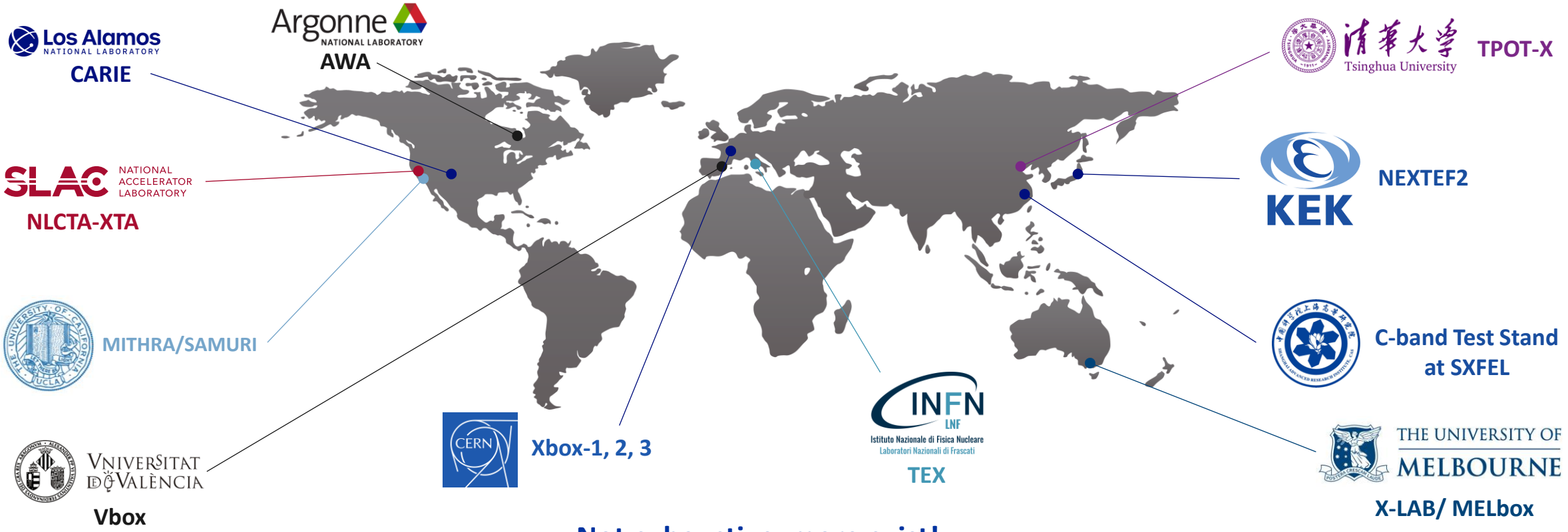

Not exhaustive, more exist!

For more see this talk from L. Wroe: https://indico.cern.ch/event/1291157/contributions/5890088/

The Early Days - Electric Field and Frequency

In 1953, Kilpatrick collated the early experimental data and offered an expression for the breakdown threshold[1]:

Reformulated in 1982 by T. J. Boyd to give the well-known **Kilpatrick Limit[2]:**

$$f = 1.64 \cdot E(MV/m)^2 \cdot e^{-8.5/E(MV/m)}\ MHz$$

Kilpatrick already noted that the limit could be increased by conditioning.

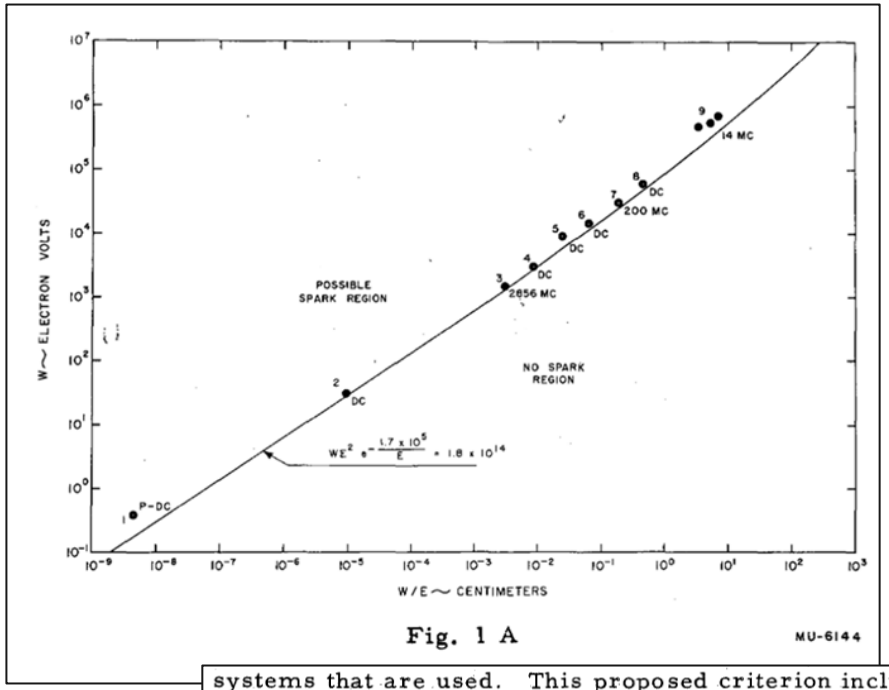

Fig. 1 A MU-6144

systems that are used. This proposed criterion includes r.f., d.c., and pulsed d.c; and determines a threshold below which no sparks should be observed during or prior to conditioning procedures. Furthermore, the boundary values plotted in Figs. 1-A and 1-B are a lower limit in the sense that they may be raised by conditioning procedures such as outgassing, cleaning the electrodes, or spark clean-up.

[1]W. Kilpatrick, "Criterion for Vacuum Sparking Designed to Include Both rf and dc", The Review of Scientific Instruments, vol. 28, pp. 824–826, 19
[2]T. J. Boyd, Jr. , "Kilpatrick's criterion", Los Alamos Group AT-1 report AT-1:82-28, February 12, 1982

Electric Field and Frequency

Proceedings of the 1986 International Linac Conference, Stanford, California, USA

VOLTAGE BREAKDOWN AT X-BAND AND C-BAND FREQUENCIES

E. TANABE
Varian Associates, Inc.
Palo Alto, California 94303

J. W. WANG and G. A. LOEW
Stanford Linear Accelerator Center
Stanford University, Stanford, California 94305

Figure 1 shows the Kilpatrick criterion with several recent experimental results obtained by various investigators, shown in Table 1.[4,5,6] These experimental studies also indicate that the breakdown threshold level increases with the frequency.

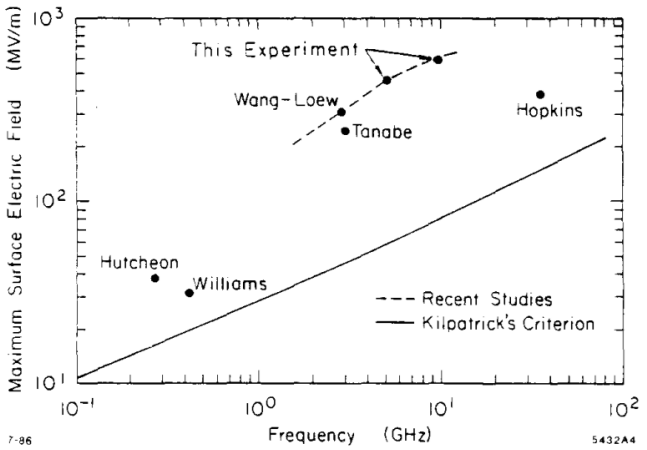

Fig. 1. Kilpatrick breakdown criterion and some experimental results.

VOLUME 90, NUMBER 22 PHYSICAL REVIEW LETTERS week ending 6 JUNE 2003

Frequency and Temperature Dependence of Electrical Breakdown at 21, 30, and 39 GHz

H. H. Braun, S. Döbert, I. Wilson, and W. Wuensch*
European Organization for Nuclear Research (CERN), CH 1211 Geneva 23, Switzerland
(Received 1 July 2002; published 5 June 2003)

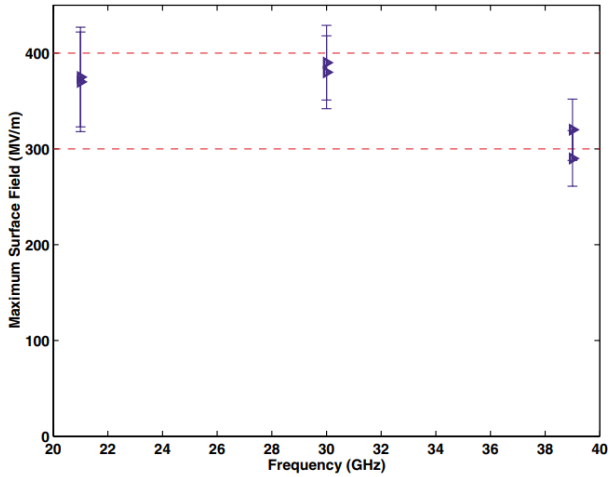

FIG. 4 (color online). Frequency dependence of the maximum surface field.

Later studies - no increase in the achievable gradient at higher frequencies. Similar result with recent S-band and C-band tests[3].

[3]M. Schneider et al., Appl. Phys. Lett. 121, 254101 (2022)

Dependence on the Electric Field

A 2009 meta-analysis of 12-30 GHz high-gradient test data → $BDR(per\ pulse) \propto E^{30}$

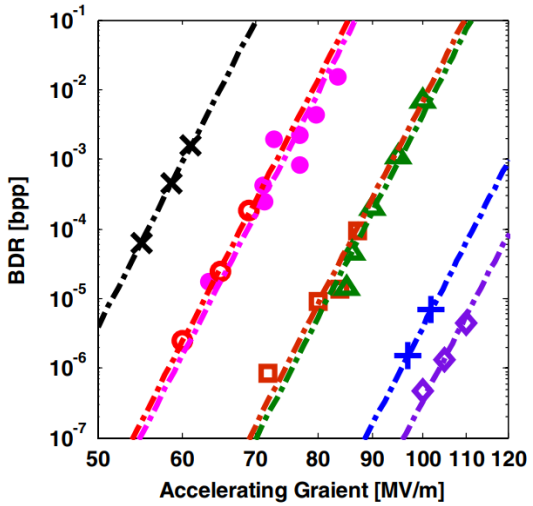

FIG. 1. (Color) Measured dependence of BDR versus gradient and the power fit for the structure number 19—(×), 10—(○), 20—(●), 4—(□), 17—(▲), 8—(+), and 3—(◇) from Table I.

A. Grudiev, S. Calatroni, and W. Wuensch, Phys. Rev. ST Accel. Beams 12,102001 (2009)

A more recent measurement, from 2025...

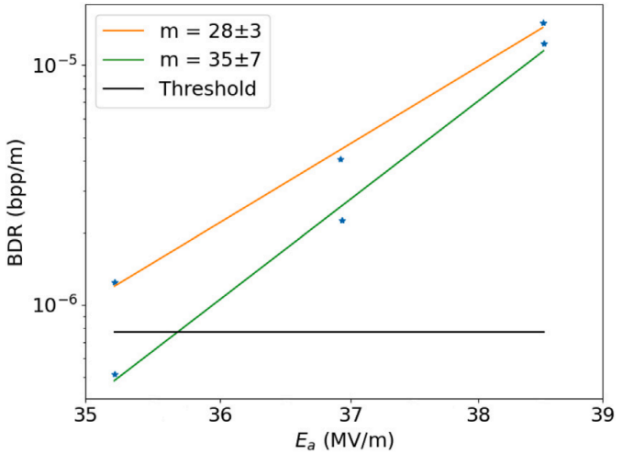

Fig. 11. BDR measurements done just after finishing the conditioning process (orange) and after 92×10^6 pulses operating at the maximum power reached (green). (For interpretation of the references to colour in this figure legend, the reader is referred to the web version of this article.)

P. Martinez-Reviriego, et al., Nucl. Eng. Tech. 57, 103164 (2025)

Investigating the Role of Power Flow

Group Velocity, V_g

2001

$$P_{abs} \sim \frac{v_g^2}{(R/Q)^2} \frac{\sin(\varphi)}{\varphi \sin(\varphi) + 2 v_g \cos(\varphi)} \text{Gradient}^2$$

where R is the cell shunt impedance, Q is the cell quality factor, and φ is the phase advance per cell. Only v_g varies significantly along the 1.8-m structures, so if damage is directly related to absorbed power, the gradient at which a given level of damage occurs scales as the inverse of v_g.

C. Adolphsen, 2001 Particle Accelerator Conference, Chicago, Il (SLAC–PUB–8901)

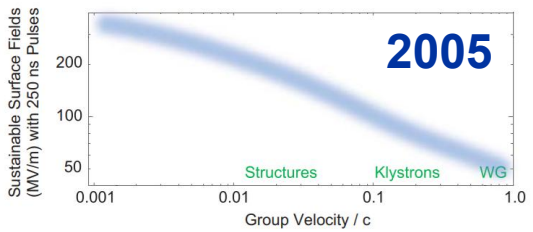

2005

C. Adolphsen, 21st IEEE Particle Accelerator Conference, Knoxville, TN, USA (2005)

P/C

The Scaling of the Traveling-Wave RF Breakdown Limit

W. Wuensch

2006

Abstract

The accelerating gradient limit given by rf breakdown in normal conducting traveling-wave structures has been observed to variously depend on a number of parameters including surface electric field, pulse length, power flow and group velocity. In order to try to empirically determine a general scaling of the breakdown limit, data has been assembled from many types of structures over the frequency range of 3 to 30 GHz. To a compelling precision, the limit appears to be given by the quantity,

$$\frac{P\tau^{1/3}}{C}$$

where P is the power flow through the structure, τ is the pulse length and C is the minimum circumference of the structure. The possible physical significance of this quantity is discussed.

S_C

New local field quantity describing the high gradient limit of accelerating structures

A. Grudiev, S. Calatroni, and W. Wuensch
CERN, CH-1211 Geneva-23, Switzerland
(Received 28 January 2009; published 26 October 2009)

2009

A new local field quantity is presented which gives the high gradient performance limit of accelerating structures due to vacuum rf breakdown. The new field quantity, a modified Poynting vector S_c, is derived from a model of the breakdown trigger in which field emission currents from potential breakdown sites cause local pulsed heating. The field quantity S_c takes into account both active and reactive power flow on the structure surface. This new quantity has been evaluated for many X-band and 30 GHz rf tests, both traveling wave and standing wave, and the value of S_c achieved in the experiments agrees well with analytical estimates.

$$S_C = Re\{\bar{S}\} + g_c \cdot Im\{\bar{S}\}$$

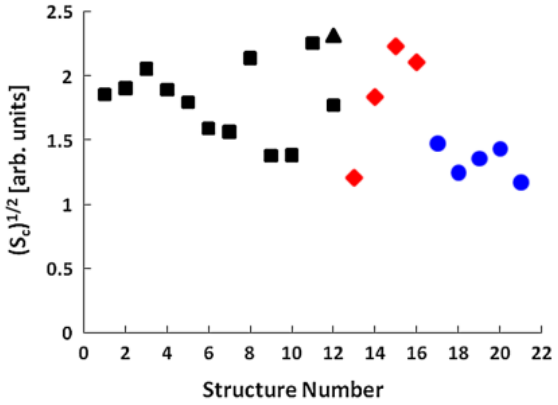

FIG. 12. (Color) Square root of S_c is plotted for the data presented in Fig. 3.

A Visual Comparison – CLIC Crab Cavity

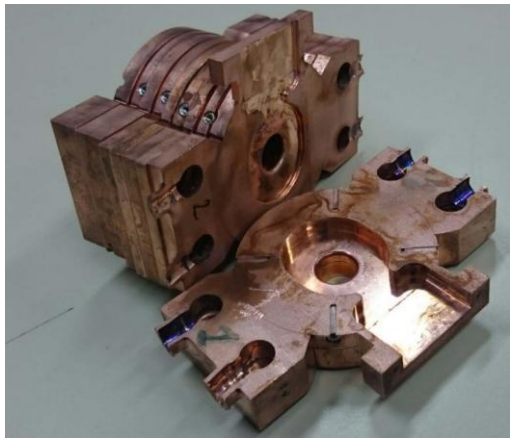

Taken from E. Rodríguez Castro's talk: https://indico.cern.ch/event/449801/contributions/1945273/

Breakdown locations shown by dots (1681 total sites).

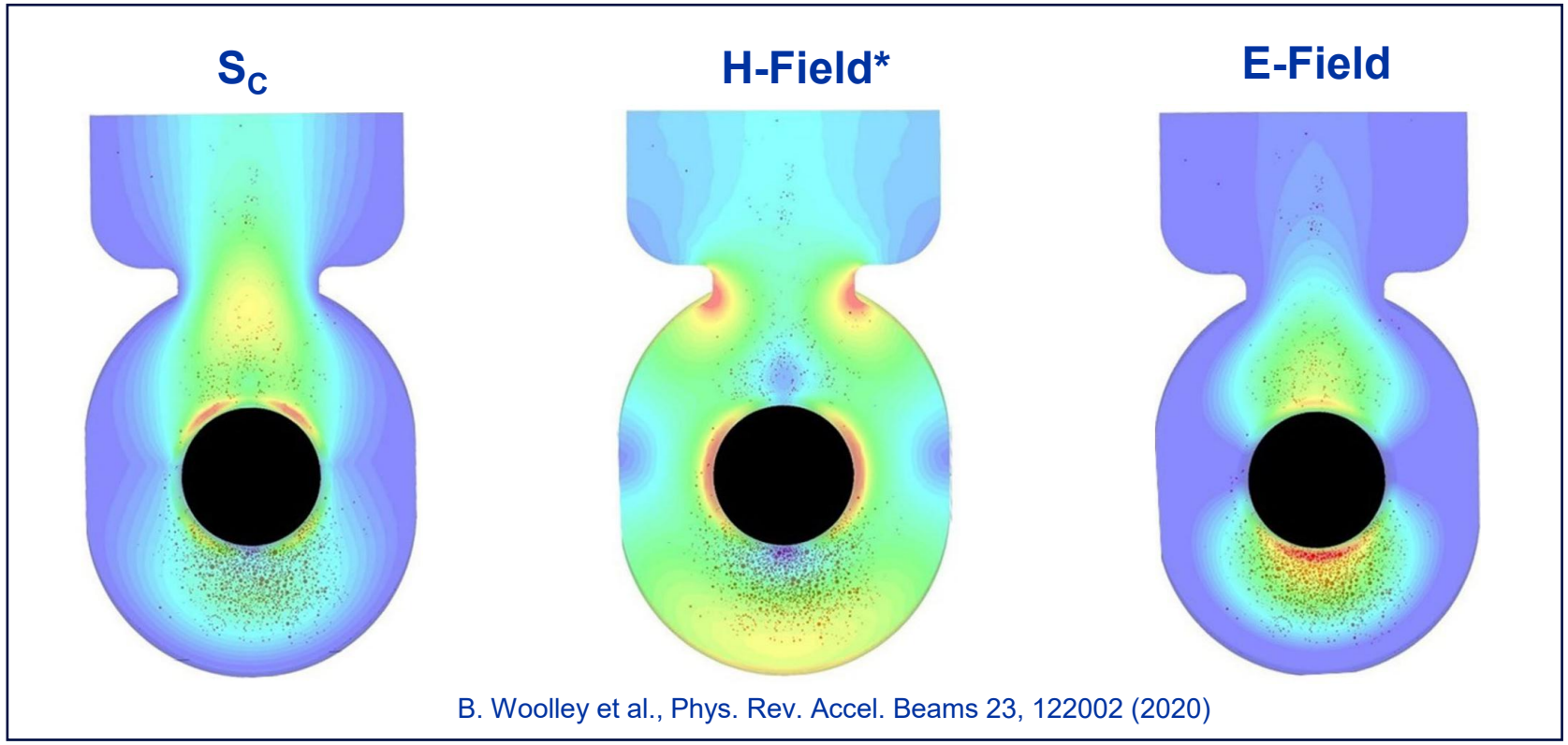

B. Woolley et al., Phys. Rev. Accel. Beams 23, 122002 (2020)

Note: Similar peak magnetic fields have been observed between structures, for example: V. Dolgashev, S. Tantawi, Y. Higashi, B. Spataro, Applied Physics Letters 97, 171501 (2010)

A Recent Addition – *E**

The breakdown-loaded electric field (*E**)

Local power coupling as a predictor of high-gradient breakdown performance

Jan Paszkiewicz,* Alexej Grudiev, and Walter Wuensch
CERN, CH-1211, Geneva 23, Switzerland
(Dated: October 3, 2022)

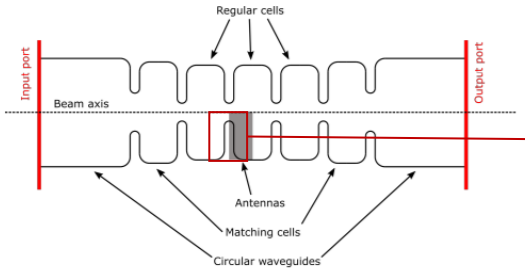

FIG. 8. Diagram of the full structure simulated. The shaded area represents the region in which antennas were placed for calculating R_{bd}.

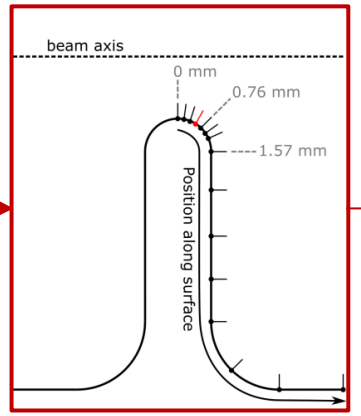

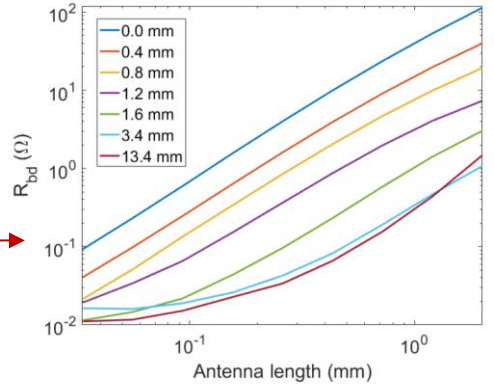

FIG. 9. Calculated R_{bd} in Ω vs. antenna length in mm for antennas in different locations in a C3 structures of 4 mm aperture radius. The distance of the antenna from the iris apex, as shown in Fig. 7, is indicated in the legend.

For a more thorough explanation, see Jan's thesis & talks:

- https://inspirehep.net/literature/2066435
- https://indico.cern.ch/event/774138/contributions/3507942/
- https://indico.global/event/4706/contributions/39379/

The Probabilistic Behaviour of Arcs

Examining the number of pulses between breakdowns (*n*), a two-rate model was fit to both RF and DC tests:

$$PDF(n) = A \cdot e^{-\alpha n} + B \cdot e^{-\beta n}$$

Classification of *primary* (Poissonian) and *secondary (or "follow-up")* breakdowns.

BDR sometimes reported for both:

- *A. D. Cahill, J. B. Rosenzweig, V. A. Dolgashev, S. G. Tantawi, S. Weathersby, Phys. Rev. Accel. Beams 21, 102002 (2018)*
- *W. L. Millar, et al., IEEE Trans.Nucl.Sci. 70 (2023) 1, 1-19 (2023)*

RF Cavity Test

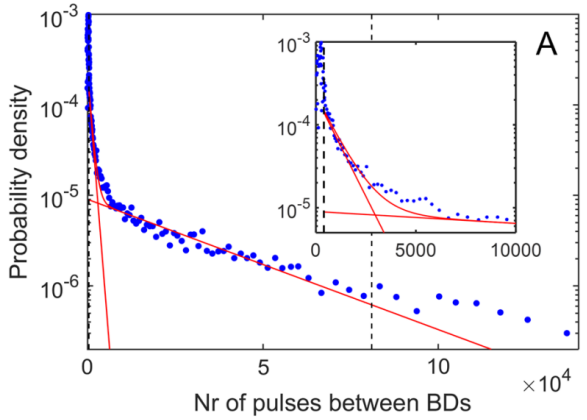

FIG. 5. Distribution of number of pulses between breakdowns and two-exponential fit, data set A. Inset shows a zoom-in of the start of the distribution.

DC Electrode Test

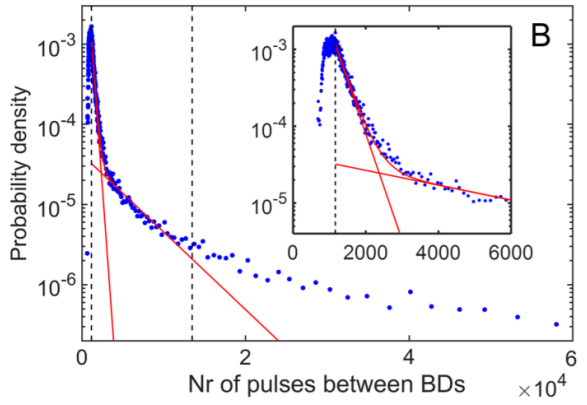

FIG. 6. Distribution of number of pulses between breakdowns and two-exponential fit, data set B. Inset shows a zoom-in of the start of the distribution.

Figures taken from: W. Wuensch, A. Degiovanni, S. Calatroni, A. Korsbäck, F. Djurabekova, R. Rajamäki, and J. Giner-Navarro, Phys. Rev. Accel. Beams 20, 011007 (2017)

Pulse Length (τ)

Back to the aforementioned meta-analysis (*Phys. Rev. ST Accel. Beams 12, 102001*):

$$BDR(per\ pulse) \propto E^{30} \cdot \tau^{5}$$

Intrinsically linked to pulsed heating and fatigue* (other limitations in their own right) but today I will focus on arcing.

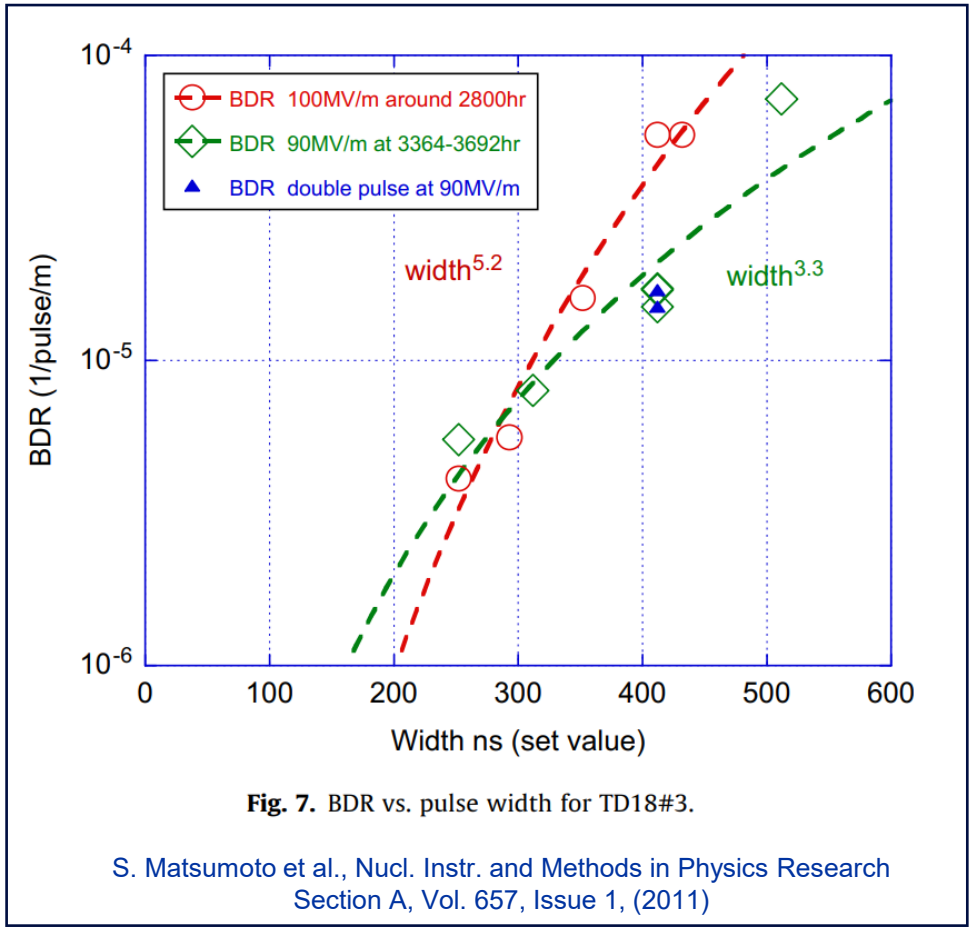

Fig. 7. BDR vs. pulse width for TD18#3.

S. Matsumoto et al., Nucl. Instr. and Methods in Physics Research Section A, Vol. 657, Issue 1, (2011)

*For a comprehensive fatigue-centric study, see: L. Laurent, et al., Phys. Rev. ST Accel. Beams 14, 041001 (2011)

Taking Advantage of the Pulse Length Scaling

Distributed Coupling Schemes*

60 ns fill-time (standard TW design).

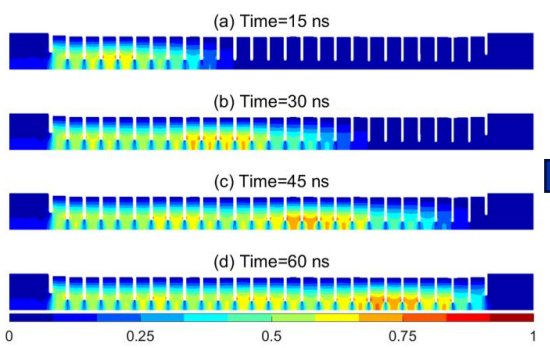

FIG. 11. Normalized temporal E_z distribution of a CLIC-T24 structure with a 60-ns input pulse.

10 ns with distributed coupling scheme.

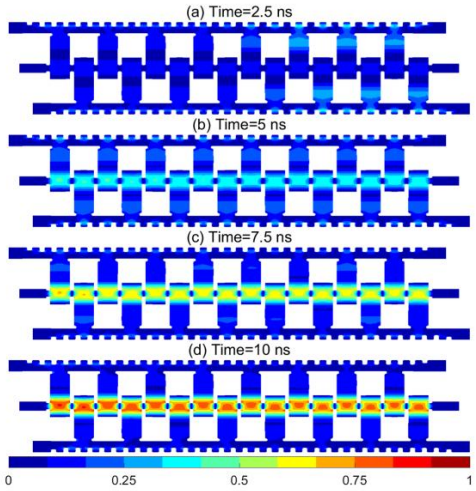

FIG. 12. Normalized temporal E_z distribution of the designed parallel-coupled structure with a 1.1-GW, 10-ns input pulse.

Figures taken from: Y. Jiang, J. Shi, H. Zha, J. Liu, X. Lin, and H. Chen, Phys. Rev. Accel. Beams 24, 112002 (2021)

* For another example, see: S. Tantawi, M. Nasr, Z. Li, C. Limborg, and P. Borchard, Phys. Rev. Accel. Beams, vol. 23, p. 092001 (2020).

Short-Pulse Machines

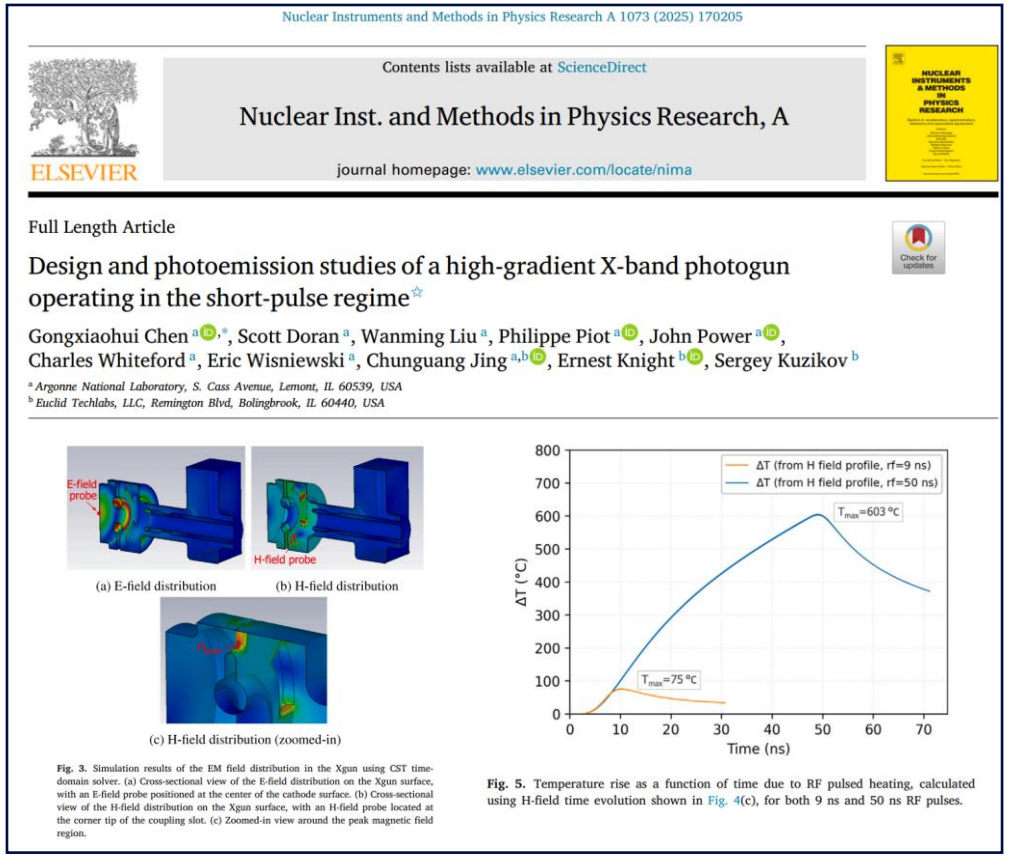

Nuclear Instruments and Methods in Physics Research A 1073 (2025) 170205

Contents lists available at ScienceDirect

Nuclear Inst. and Methods in Physics Research, A

journal homepage: www.elsevier.com/locate/nima

Full Length Article

Design and photoemission studies of a high-gradient X-band photogun operating in the short-pulse regime☆

Gongxiaohui Chen [a],*, Scott Doran [a], Wanming Liu [a], Philippe Piot [a], John Power [a], Charles Whiteford [a], Eric Wisniewski [a], Chunguang Jing [a,b], Ernest Knight [b], Sergey Kuzikov [b]

[a] Argonne National Laboratory, S. Cass Avenue, Lemont, IL 60539, USA
[b] Euclid Techlabs, LLC, Remington Blvd, Bolingbrook, IL 60440, USA

(a) E-field distribution (b) H-field distribution

(c) H-field distribution (zoomed-in)

Fig. 3. Simulation results of the EM field distribution in the Xgun using CST time-domain solver. (a) Cross-sectional view of the E-field distribution on the Xgun surface, with an E-field probe positioned at the center of the cathode surface. (b) Cross-sectional view of the H-field distribution on the Xgun surface, with an H-field probe located at the corner tip of the coupling slot. (c) Zoomed-in view around the peak magnetic field region.

Fig. 5. Temperature rise as a function of time due to RF pulsed heating, calculated using H-field time evolution shown in Fig. 4(c), for both 9 ns and 50 ns RF pulses.

Taking Advantage of the Pulse Length Scaling

Distributed Coupling S… …ort-Pulse Machines

60 ns fill-time
(standard TW design).

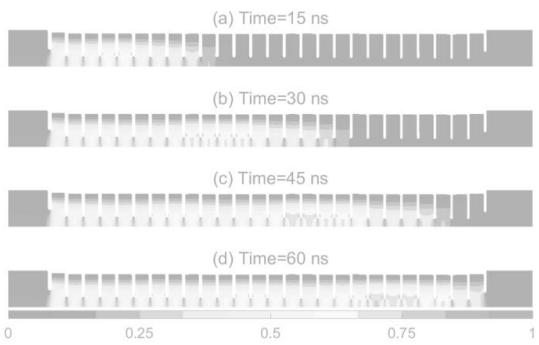

FIG. 11. Normalized temporal E_z distribution of a CLIC-T24 structure with a 60-ns input pulse.

10 …

FIG. 12. N… parallel-cou…

Figures taken from: Y. Jiang, J. Shi, H. Zha, J. Liu, X. Lin, … Rev. Accel. Beams 24, 112002 (2021)

* For another example, see: S. Tantawi, M. Nasr, Z. Li, C. Limborg, and P. Borch… 092001 (2020).

IEEE Transactions on Nuclear Science, Vol.NS-24, No.3, June 1977

PARALLEL COUPLED CAVITY STRUCTURE*

R. M. Sundelin, J. L. Kirchgessner, and M. Tigner
Laboratory of Nuclear Studies, Cornell University
Ithaca, New York 14853

Previously at Cornell University…

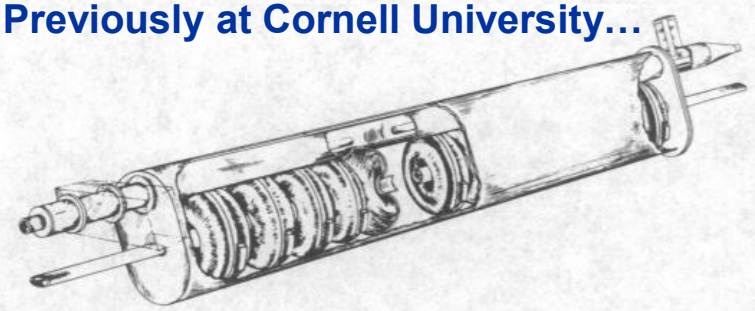

Fig. 1. Parallel coupled cavity structure, including water tank used for cooling.

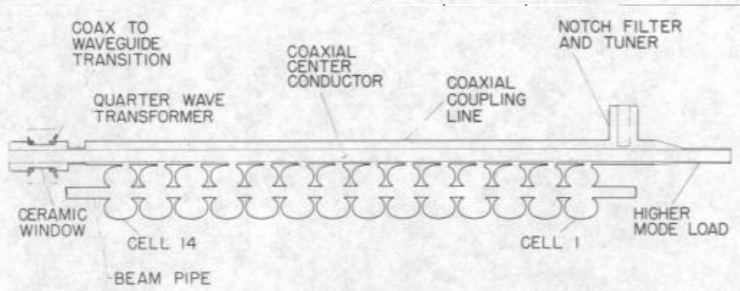

Fig. 2. Side sectional view of parallel coupled cavity structure.

Nuclear Instruments and Methods in Physics Research A 1073 (2025) 170205

Contents lists available at ScienceDirect

Nucl. Inst. and Methods in Physics Research, A

journal homepage: www.elsevier.com/locate/nima

…udies of a high-gradient X-band photogun …regime☆

…, Wanming Liu [a], Philippe Piot [a,b], John Power [a], …i [a], Chunguang Jing [a,b], Ernest Knight [b], Sergey Kuzikov [b]
…60539, USA
…440, USA

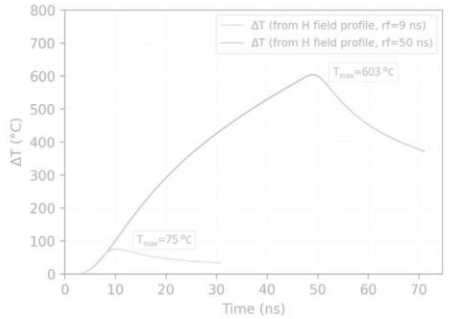

Fig. 5. Temperature rise as a function of time due to RF pulsed heating, calculated using H-field time evolution shown in Fig. 4(c), for both 9 ns and 50 ns RF pulses.

RF Material Tests

Molybdenum & Tungsten Irises (30 GHz tests)

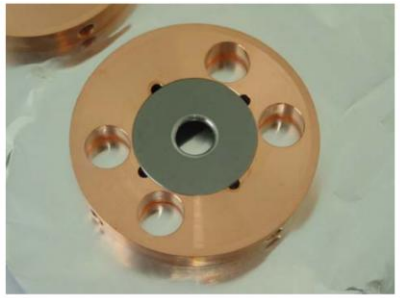

Figure 1: Tungsten-iris inserted into a copper disk forming together a cell of the rf structure.

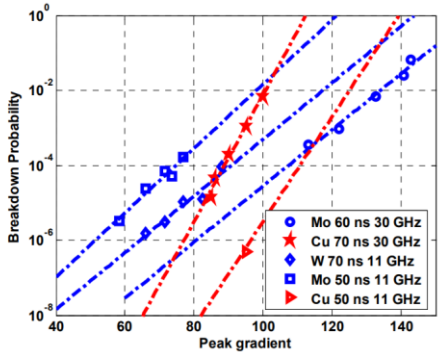

Figure 4: Break down probability as a function of gradient, for different structures.

S. Döbert, et al., CLIC-Note-699 (2006)

Copper and its Alloys

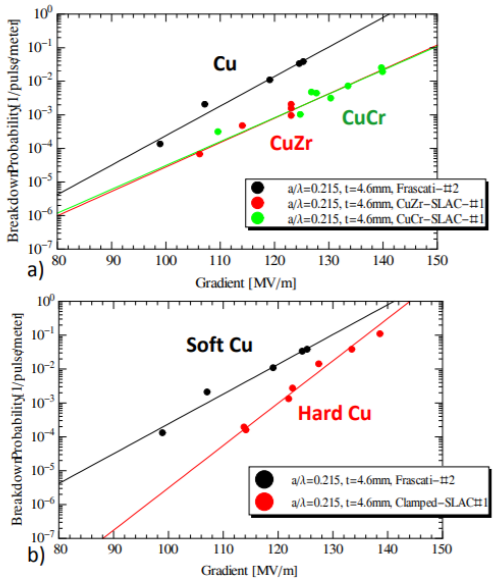

Figure 7: Comparison of SW structures made of copper and different copper alloys. Breakdown rate *vs.* gradient for brazed structures, and b) soft (brazed) and hard (clamped) copper. The data is for a shaped rf pulse with ∼ 170 ns charging time and 150 ns flat part.

V. Dolgashev, Linear Accelerator Conference LINAC2010, Tsukuba, Japan (2010)

More recently: ~25% improvement with CuAg (compared to pure Cu)

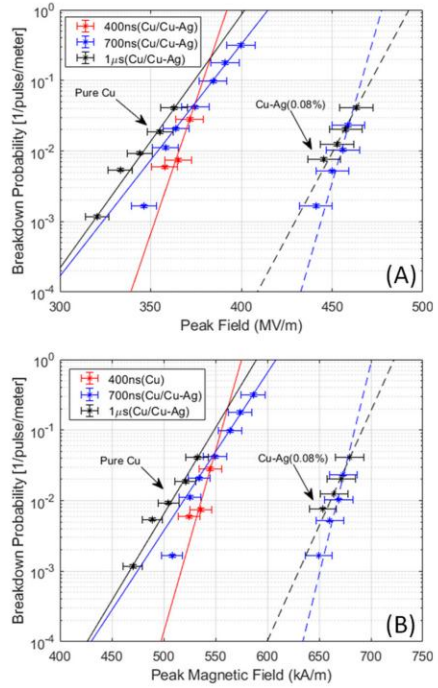

FIG. 5. BDR plotted (a) as a function of peak electric field (E_p) and (b) peak magnetic field (H_p) on the surface of the accelerator structures. The trendlines are the data fitted to an exponential fit. Note that the accuracy of the trendline is low over a large dynamic range.

M. Schneider, et al., Appl. Phys. Lett. 121, 254101 (2022)

RF Material Tests

Molybdenum & Tungsten Irises (30 GHz tests)

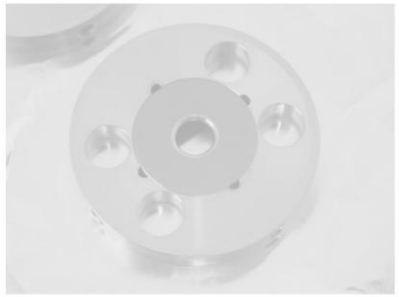

Figure 1: Tungsten-iris inserted into a copper disk forming together a cell of the rf structure.

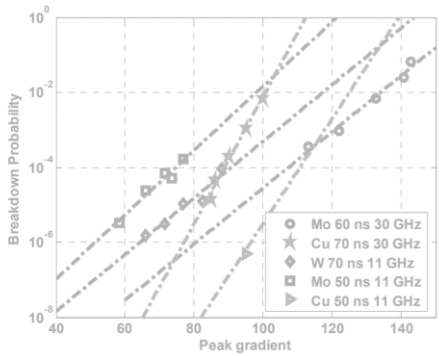

Figure 4: Break down probability as a function of gradient, for different structures.

S. Döbert, et al., CLIC-Note-699 (2006)

Even gold-plated components at 11.424 GHz!

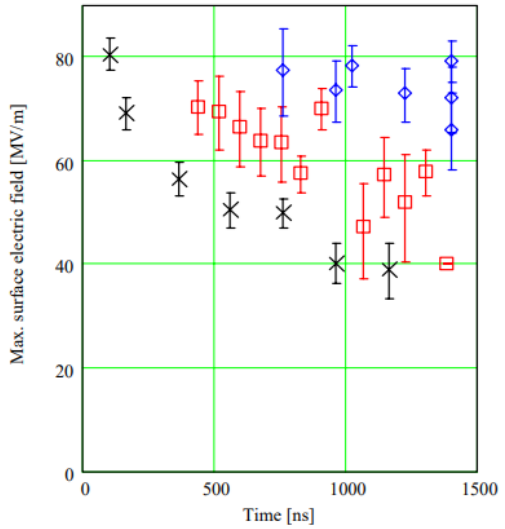

Figure 2: Maximum surface electric field *vs.* pulse length for low-magnetic-field waveguides with walls made of different materials: boxes - copper, x - gold plated, diamonds - stainless steel.

V. Dolgashev, SLAC-PUB-10355 (2004)

V. Dolgashev, Linear Accelerator Conference LINAC2010, Tsukuba, Japan (2010)

More recently: ~25% improvement with CuAg (compared to pure Cu)

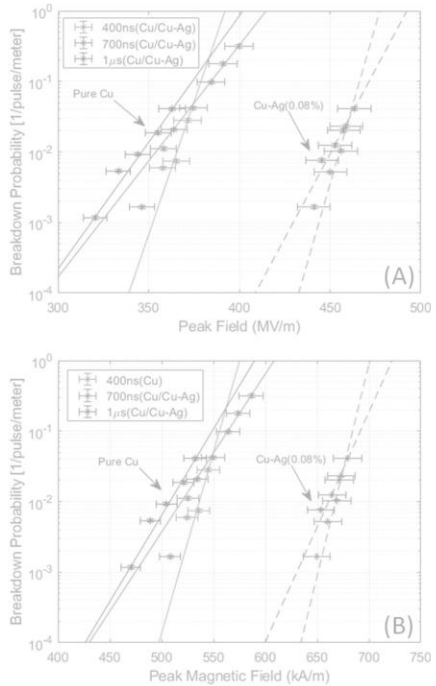

FIG. 5. BDR plotted (a) as a function of peak electric field (E_p) and (b) peak magnetic field (H_p) on the surface of the accelerator structures. The trendlines are the data fitted to an exponential fit. Note that the accuracy of the trendline is low over a large dynamic range.

M. Schneider, et al., Appl. Phys. Lett. 121, 254101 (2022)

DC Material Tests

A short DC detour – recent material tests from CERN's Large Electrode System (LES) as part of a radiofrequency quadrupole (RFQ) project. The RFQ is an H- accelerator → hydrogen deposition occurs during operation → irradiated and non-irradiated samples both tested to quantify high-field performance.

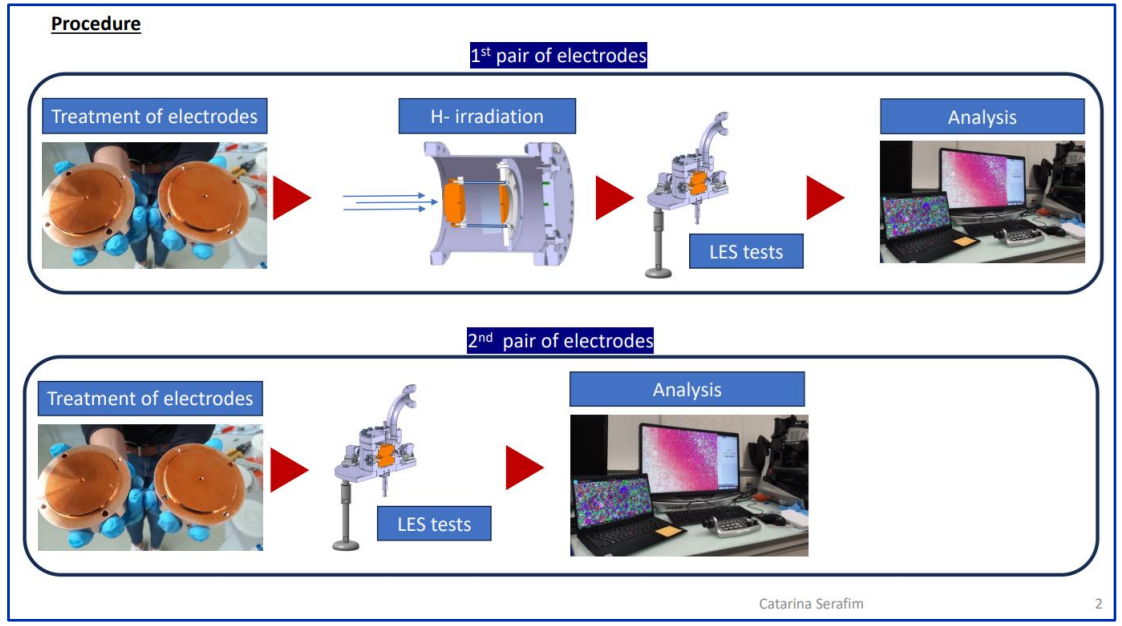

Slides taken from Catarina Serafim's MeVArc 2024 talk: https://indico.cern.ch/event/1298949/contributions/5783871

DC Material Tests

PHYSICAL REVIEW ACCELERATORS AND BEAMS **28,** 013101 (2025)

Effects of H⁻ low beam irradiation and high field pulsing tests in different metals

C. Serafim,[1,2,*] S. Calatroni,[1,†] F. Djurabekova,[2] R. Peacock,[1] V. Bjelland,[1,3] A. T. Perez-Fontenla,[1] W. Wuensch,[1] A. Grudiev,[1] S. Sgobba,[1] A. Lombardi,[1] and E. Sargsyan[1]

[1]*CERN, European Organization for Nuclear Research, 1211 Geneva, Switzerland*
[2]*Helsinki Institute of Physics and Department of Physics, P.O. Box 43, University of Helsinki, FI-00014, Finland*
[3]*Department of Physics, NTNU, 9491 Trondheim, Norway*

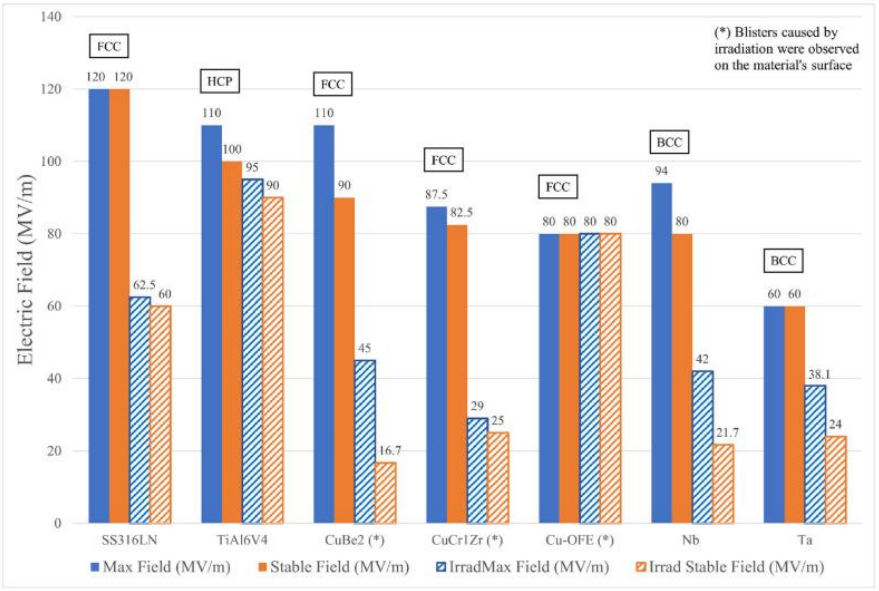

FIG. 14. Bar plot showing the results for all the tested materials in the LES system. The solid bars represent the results of nonirradiated electrodes. The lined bars represent the results for the irradiated electrodes. The blue and orange colors represent, respectively, the maximum and stable electric field achieved during testing.

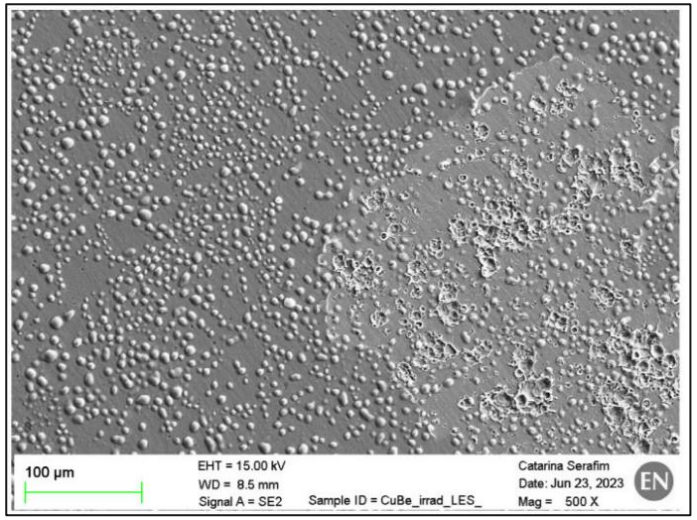

SEM image of the electrode showing blistering and breakdown craters.

Normal Conducting Materials at Low Temperatures

My last slide on DC tests - a similar setup with cryogenic capabilities at Uppsala university in Sweden.

Temperature-Dependent Field Emission and Breakdown Measurements Using a Pulsed High-Voltage Cryosystem

Marek Jacewicz,[1,*] Johan Eriksson,[1] Roger Ruber,[1] Sergio Calatroni,[2] Iaroslava Profatilova,[2] and Walter Wuensch[2]

[1] *Department of Physics and Astronomy, Uppsala University, Regementsv. 1, 75237 Uppsala, Sweden*
[2] *CERN, European Organization for Nuclear Research, CH-1211 Geneva 23, Switzerland*

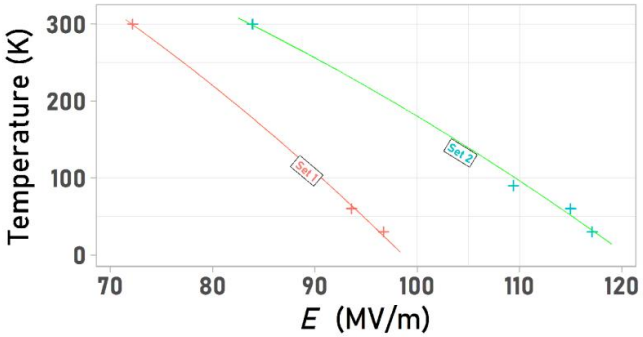

FIG. 2. Measured values of the maximum surface field at different temperatures for both sets of electrodes. The lines are the fits from the crystal defect model [Eq. (2)].

Warm-up and cooldown also investigated.

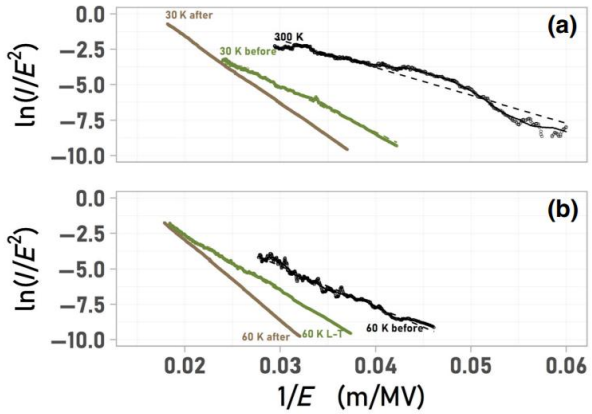

FIG. 3. (a) Field emission after conditioning at 300 K (black), cool-down to 30 K (green), and after re-conditioning at 30 K (brown). (b) FE for surface cooled down to 60 K after conditioning at 300 K (black), after re-conditioning at 60 K (brown), and compared with FE at 60 K after 9 days (green).

Normal Conducting Materials at Low Temperatures

And of course, the RF efforts…

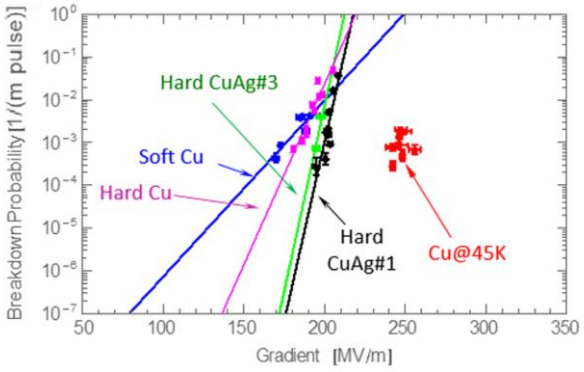

A. D. Cahill, J. B. Rosenzweig, V. A. Dolgashev, S. G. Tantawi, S. Weathersby, Phys. Rev. Accel. Beams 21, 102002 (2018)

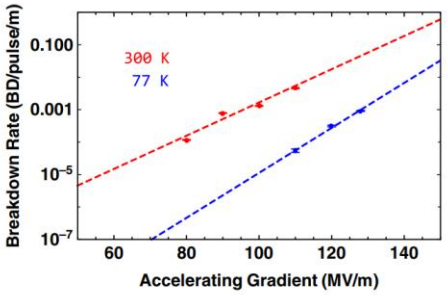

FIG. 9. The collected breakdown rates with the fitted slope of the distributed-coupling accelerator structure at 300 and 77 K. The breakdown rates at 300 K are obtained from our previous testing of the same accelerator structure at room temperature. For both operating temperatures, the data were collected for a 400 ns stepped pulse with a flat gradient of 200 ns. The results show a reduction by 2 orders of magnitude, $\times\frac{1}{100}$, in breakdown rates at the same gradient levels from 300 to 77 K operation.

M. Nasr et al., Phys. Rev. Accel. Beams 24, 093201 (2021)

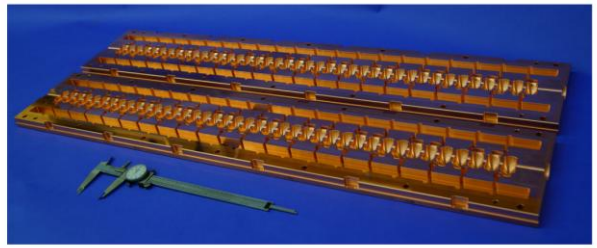

Figure 3. Both halves of the C^3 prototype structure prior to braze. The one meter structure consists of 40 cavities. A rf manifold that runs parallel to the structure feeds 20 cavities on each side. The structure operates at 5.712 GHz.

The C^3 structures will operate in a bath of LN_2 cooled to a cryogenic temperature of approximately ~ 80 K. The increased conductivity of copper at this temperature results in a shunt impedance of the optimized accelerator cavity of 300 MΩ/m, six times the effective shunt impedance of the Next Linear Collider (NLC) X-band accelerating structure.

E. A. Nanni et al., 2023 JINST 18 P09040

Normal Conducting Materials at Low Temperatures

And of course, the RF efforts…

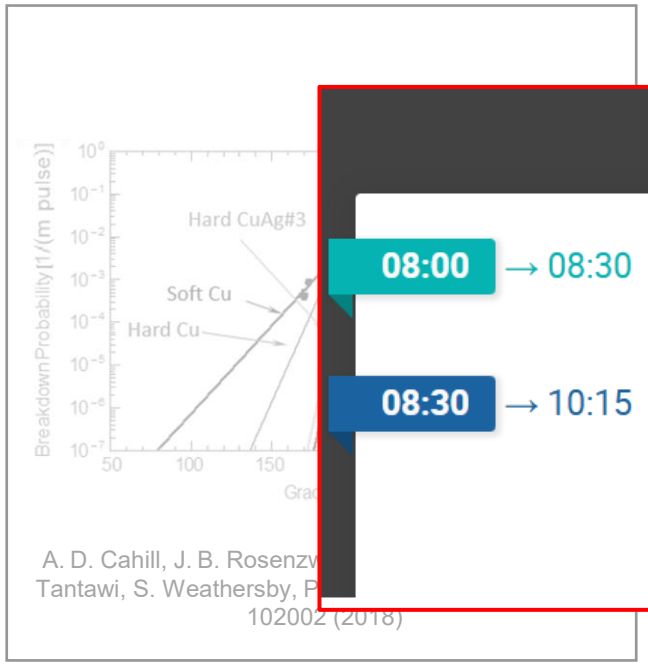

A. D. Cahill, J. B. Rosenzv
Tantawi, S. Weathersby, P
102002 (2018)

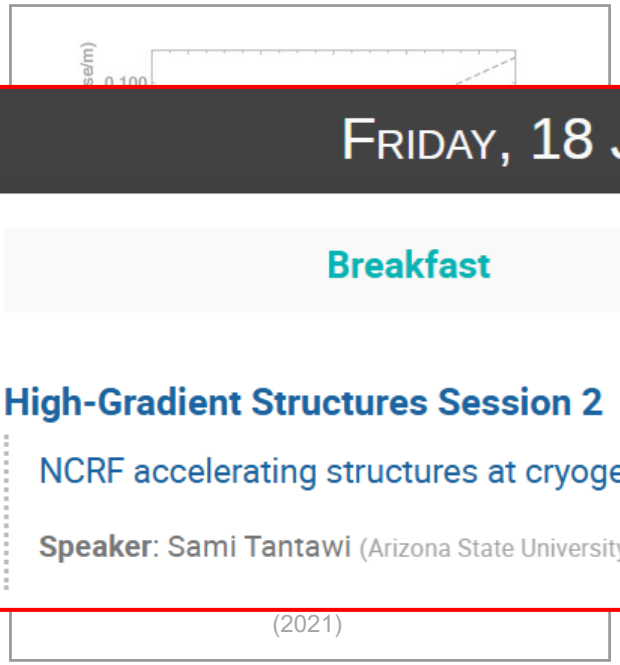

(2021)

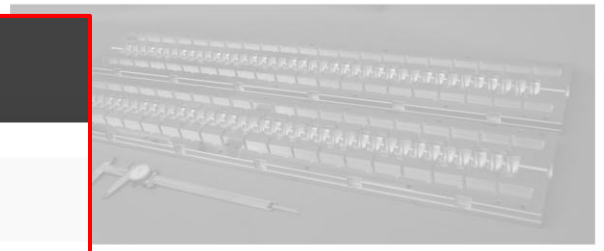

alves of the C^3 prototype structure prior to braze. The one meter structure consists of 40
ufold that runs parallel to the structure feeds 20 cavities on each side. The structure operates

of LN_2 cooled to a cryogenic temperature of approximately
oper at this temperature results in a shunt impedance of
Ω/m, six times the effective shunt impedance of the Next
g structure.

E. A. Nanni et al., 2023 JINST 18 P09040

Friday, 18 July

08:00 → 08:30 **Breakfast**

08:30 → 10:15 **High-Gradient Structures Session 2**

NCRF accelerating structures at cryogenic temperature (8:30 - 8:48) ¶

Speaker: Sami Tantawi (Arizona State University)

The Conditioning Effect (at Room Temperature)

To finish – a few words on conditioning…

- **The surface conditions (or worsens) during measurements --> the measurement order matters.**
- **What mechanism(s) is/are predominantly responsible exactly?**
- **Can we condition with substantially fewer BDs? Is there any benefit to doing so?**

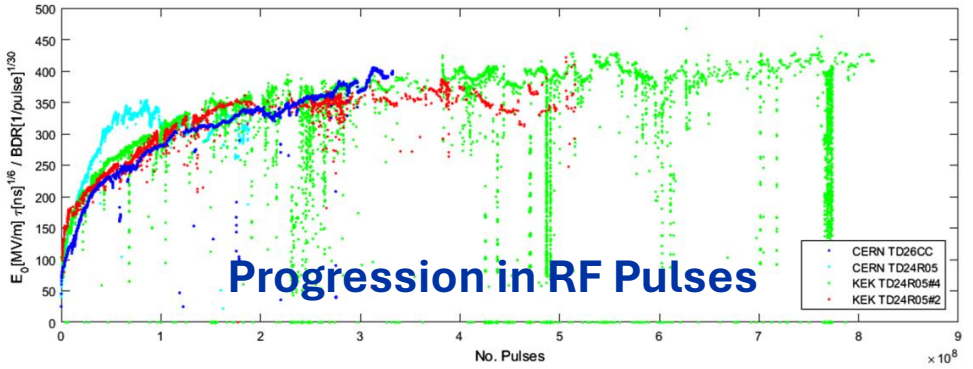

FIG. 3. Comparison of the scaled gradient vs number of accumulated pulses for several structures. Despite the different conditioning approaches, the curves for the scaled gradient are similar.

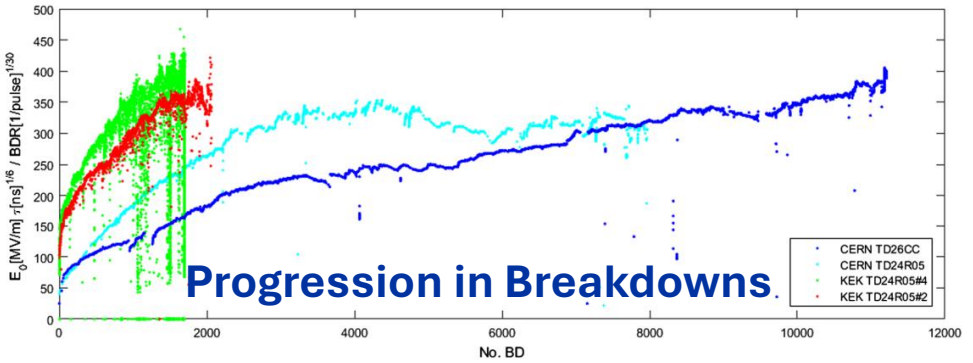

FIG. 4. Comparison of the scaled gradient vs number of accumulated breakdowns for several structures. When plotted with respect to the total accumulated number of breakdowns, the curves of the scaled gradient diverge significantly.

Taken from: A. Degiovanni, W. Wuensch, J. Giner-Navarro, Phys. Rev. Accel. Beams 19, 032001 (2016)

The Conditioning Effect (at Room Temperature)

IEEE TRANSACTIONS ON NUCLEAR SCIENCE, VOL. 72, NO. 3, MARCH 2025

Multiyear Longitudinal Analysis of Vacuum Breakdown and RF Conditioning in the C-Band Linac of SwissFEL

Thomas G. Lucas, Jürgen Alex, Carl Beard, Alessandro Citterio, Hans-Heinrich Braun, Paolo Craievich, *Senior Member, IEEE*, Zheqiao Geng, Roger Kalt, Florian Loehl, Marco Pedrozzi, Jean-Yves Raguin, and Riccardo Zennaro

>100 C-band structures operating at ~ 30 MV/m.

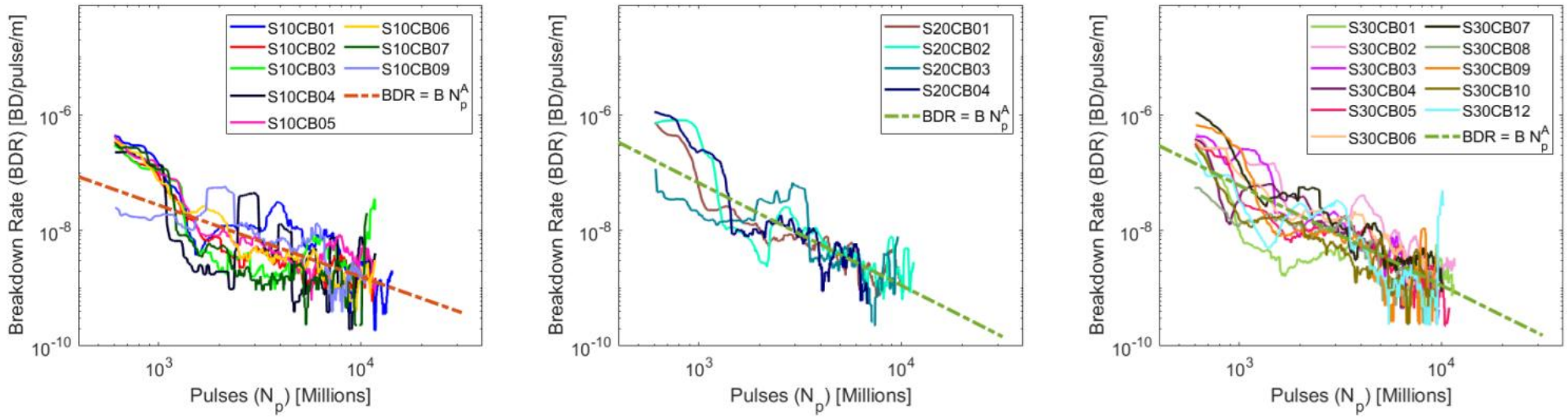

Fig. 9. Vacuum breakdown rate against the cumulative number of RF pulses during the user operation. This is plotted for approximately 9400 million RF pulses, which equates to around three years of continuous operation at an RF pulse repetition rate of 100 Hz. Each is fit with an inverse power law of the form $BDR = BN_p^A$.

Conclusions

- **We now have a plethora of experiments (and models) that show how structures perform and what the main dependencies are → can be used to inform design choices and optimise a given device.**
- **Promising options are being investigated, including short pulse machines, more "resilient" metals, and operation at cryogenic temperatures.**
- **A word of caution - conditioning is a dynamic phenomenon, care must be taken when interpreting some of these breakdown-related test results!**

A final acknowledgement – for more on any particular aspect, I direct you to the workshops on the right. Much of the content in this presentation originated from these communities!

https://indico.fnal.gov/event/65159/

https://indico.slac.stanford.edu/event/9387/overview

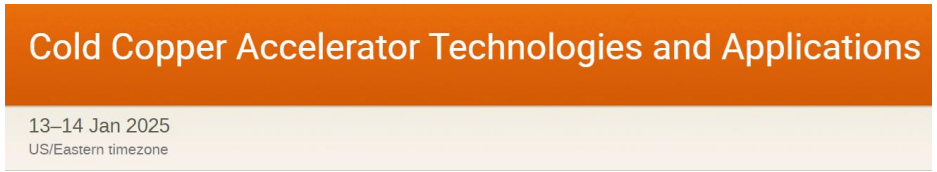

https://indico.cern.ch/event/1424597/

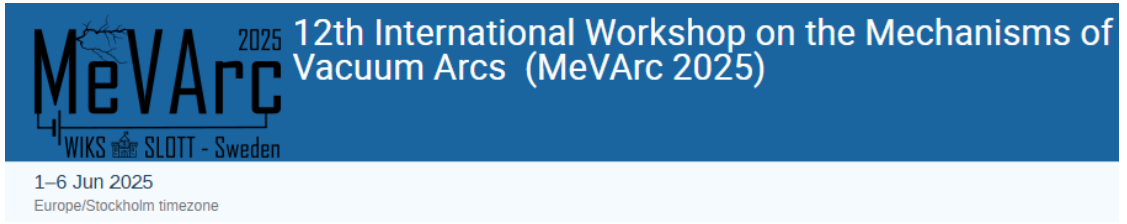

And a recent review and consolidation of much of the experimental and theoretical work from the members: https://arxiv.org/abs/2502.03967

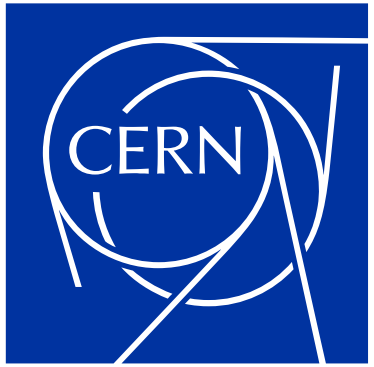

home.cern